WPMAT-CPR(17) 17104

K Mergia et al.

Comparative Study of the Mechanical Properties of Different Tungsten Materials for Fusion Applications

Preprint of Paper to be submitted for publication in Proceeding of 16th International Conference on Plasma-Facing Materials and Components for Fusion Applications

This work has been carried out within the framework of the EUROfusion Consortium and has received funding from the Euratom research and training programme 2014-2018 under grant agreement No 633053. The views and opinions expressed herein do not necessarily reflect those of the European Commission.

Physica Scripta

PAPER

Comparative study of the mechanical properties of different tungsten materials for fusion applications

To cite this article: S Krimpalis *et al* 2017 *Phys. Scr.* **2017** 014068

IOP Publishing | Royal Swedish Academy of Sciences Physica Scripta

Phys. Scr. **T170** (2017) 014068 (8pp) https://doi.org/10.1088/1402-4896/aa9292

Comparative study of the mechanical properties of different tungsten materials for fusion applications

S Krimpalis[1], K Mergia[1], S Messoloras[1], A Dubinko[2,3], D Terentyev[2], K Triantou[1], J Reiser[4] and G Pintsuk[5]

[1] National Centre for Scientific Research, 'Demokritos', Institute of Nuclear and Radiological Science and Technology, Energy and Safety, 15310 Aghia Paraskevi, Athens, Greece
[2] SCK·CEN, Institute for Nuclear Material Sciences, B-2400 Mol, Belgium
[3] Department of Applied Physics, Ghent University, B-9000 Ghent, Belgium
[4] Karlsruhe Institute of Technology (KIT), Institute for Applied Materials, D-76344 Eggenstein-Leopoldshafen, Germany
[5] Forschungszentrum Jülich GmbH, EURATOM Association, D-52425 Jülich, Germany

E-mail: kmergia@ipta.demokritos.gr

Received 26 May 2017, revised 10 October 2017
Accepted for publication 11 October 2017
Published 28 November 2017

Abstract

The mechanical properties of tungsten produced in different forms before and after neutron irradiation are of considerable interest for their application in fusion devices such as ITER. In this work the mechanical properties and the microstructure of two tungsten (W) products with different microstructures are investigated using depth sensing nano/micro-indentation and transmission electron microscopy, respectively. Neutron irradiation of these materials for different doses, in the temperature range 600 °C–1200 °C, is underway within the EUROfusion project in order to progress our basic understanding of neutron irradiation effects on W. The hardness and elastic modulus are determined as a function of the penetration depth, loading/unloading rate, holding time at maximum load and the final surface treatment. The results are correlated with the microstructure as investigated by SEM and TEM measurements.

Supplementary material for this article is available online

Keywords: tungsten, nanoindentation, TEM, hardness, elastic modulus

(Some figures may appear in colour only in the online journal)

1. Introduction

Tungsten (W) is a candidate plasma facing material for fusion reactors due to its high melting point, high thermal conductivity, low tritium retention, good sputtering resistance, low swelling, thermal stress and shock resistance and high temperature strength [1, 2]. However, it suffers from brittle behavior at low temperatures, due to the relatively high brittle to ductile transition temperature ranging from room temperature to several hundreds of degrees Celsius [2], and this causes a limitation of its exploitation. Several methods of microstructure modification [3–7] have been proposed to cope with the low toughness problem. In a fusion device neutrons are produced through the deuterium–tritium reaction, which is the most efficient fusion reaction, and when they impinge on a material they cause different effects which change its performance. Within the framework of the EUROfusion project WPMAT [8] neutron irradiation of these materials for different doses, in the temperature range 600 °C–1200 °C, of tungsten materials is underway in order to advance the understanding of the basic phenomena underlying the neutron irradiation effects on tungsten and provide experimental validation of theoretical models. As a first step towards this goal it is crucial to obtain reference data of the non-irradiated materials.

Table 1. Material description.

Material	Description	Surface treatment of indentation samples
'Cold rolled' W sheet-A 1 mm thickness purity >99.97%	Heavily deformed low temperature rolling sheet (below 1200 °C) and stress relief annealing [17]	Chemomechanical polishing with colloidal silica containing 5% CrO_3 aqueous solution (20 g in 100 ml water)
'Cold rolled' W sheet-B 1 mm thickness purity >99.97%	Heavily deformed low temperature rolling sheet (below 1200 °C) and stress relief annealing [17]	Electropolishing at 20 V in 4% aqueous solution of NaOH
W forged bar 36 × 36 mm^2 cross section purity >99.97%	Fabrication by forging/hammering from two orthogonal directions	Electropolishing at 20 V in 4% aqueous solution of NaOH

Nowadays, nano-indentation is widely used for the study of the mechanical properties of materials on the nano-scale because of the ease, speed and sample simplicity with which it can be carried out [9]. Its major advantage stems from the fact that the fabrication of specific sample geometries required in the traditional methods is avoided and small masses and volumes can be used. Also the development of nanomaterial science and nanotechnology has caused the demand for the determination of the mechanical properties at the nano-level. However, there is a question if the results are representative of bulk volumes and indentation tests at macro-level may resolve the issue. Current technologies allow the accurate measurement of loads as low as 0.1 μN and displacements of about 0.1 nm. Several works report on the use of nano-indentation for determining the mechanical properties of tungsten [10–15]. In the current work the nano-indentation is utilized as a method for determining the mechanical properties of tungsten material in order to decrease the required mass of the materials under neutron irradiation since the long term aim of the project is to assess the neutron irradiation effects on the mechanical properties of tungsten.

The mechanical properties of materials depend strongly on their microstructure and to this end two classes of W material are investigated, namely, cold-rolled tungsten in sheet form and tungsten in forged bar form. The justification behind the selection of these materials lies on the fact that (a) it has been shown that cold-rolling is a process which increases the ductility and strength of W at room temperature [16] and (b) the forged bar material is one of the options of the plasma facing material for ITER and the best characterized tungsten grade in Europe in terms of mechanical, thermo-physical and high heat flux properties [17].

In the current study, by employing depth sensing nano-indentation, the values of hardness (H) and elastic modulus (E) of the two tungsten materials are determined and the influence of indentation depth, loading and unloading rates and holding time at the maximum load are discussed and correlated with the microstructure.

2. Materials and methods

Two types of tungsten (W) materials are investigated in the current study, namely low temperature rolling 1 mm thick W sheet (details can be found in [18]) and W forged bar, as described in table 1. The W materials in sheet and bar form are both produced by PLANSEE SE in a powder metallurgical route consisting of sintering and rolling or hot forging from two orthogonal directions. Tungsten produced by rolling has a plate-like grain shape while forging results in a uniaxial elongated grain shape [17].

Scanning electron microscopy (SEM) measurements were carried out using a FEI instrument. The specimens were cut from the raw material in disk form, as described below for the indentation measurements, and were subsequently mechanically polished, electropolished at 20 V in a 4% aqueous solution of NaOH and finally etched at 3 V using an etchant consisting of 25 cc of a normal solution of NaOH and 20 cc of H_2O_2.

The specimens for the TEM samples, regarding the W forged bar, were cut from the middle such that the elongated grains are contained within the sample (not normal to it). The TEM specimens of the W sheet were obtained from 12 mm diameter disks cut from the original 1 mm thick sheet. For each material at least three samples were investigated. All specimens were mechanically polished from both sides using SiC paper to achieve 70–100 μm thickness and further cut with a wire cutter into pieces to fit 3 mm TEM grids. They were polished again from both sides with 4000 grit SiC paper to remove the remnants of a glue, rinsed in acetone and ethanol and then glued on 3 mm copper grids with an aperture of 1 mm. Finally, TEM specimens were polished electrochemically with a solution of 1.5 wt% NaOH in water with applied voltage of 30 V. The specimens were investigated with JEOL 2010 TEM operating at 200 kV and JEOL 3010 TEM operating at 300 kV. The TEM images were taken using bright condition to enhance resolution of dislocation lines in the same style as presented in figures 2 and 3. The average dislocation density was measured following the methodology used in [19]. For each material at least twenty grains were measured. Each calculation requires a TEM micrograph, corresponding diffraction pattern and convergent beam electron diffraction (CBED) pattern. Several calculations at different areas of the specimen were performed to get an average number of dislocation density. In Digital Micrograph software, provided with the image sensor of a microscope, a circle is drawn randomly in an image and the number of intersections of it with dislocation lines is counted. Dislocation density is then

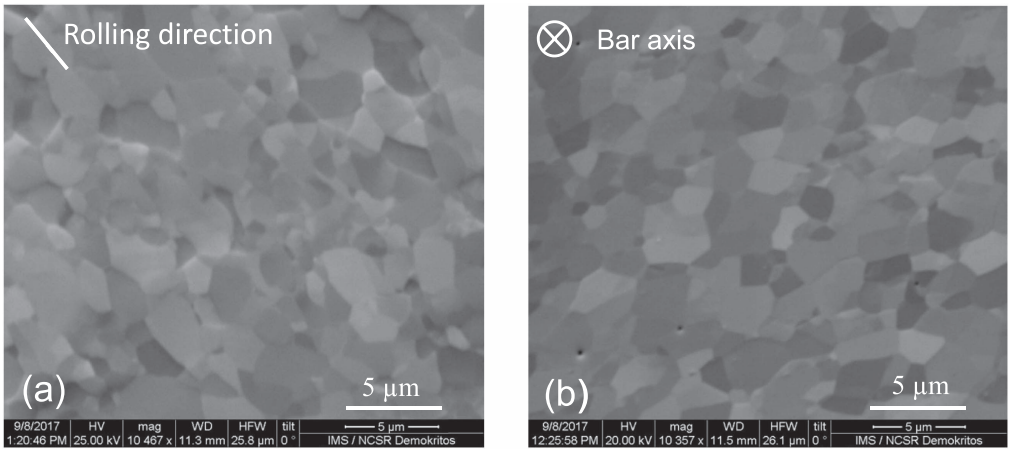

Figure 1. SEM image of the W microstructure in (a) sheet and (b) forged bar form.

calculated as $\rho = 2N/Lt$, where N is the number of intersections of the circle with dislocation lines, L—the circumference of the circle, t—local thickness of the specimen at the area of the image. The length of the circle is automatically calculated in the Digital Micrograph software. The local thickness of the specimen is determined from the CBED pattern and diffraction pattern.

For the indentation measurements disks with thickness of about 1 mm and diameter around 12 mm were sectioned which were subsequently mechanically polished using diamond suspension to obtain mirror quality surface. The disks sectioned from the W forged bar were cut from 36 × 36 mm^2 slices of the bar having their surface normal along the bar axis. The final step of the surface treatment of the investigated materials for the measurement of the mechanical properties is presented in table 1. For the 'cold rolled' W sheet both electropolishing and chemomechanical polishing were employed in order to assess the effect of surface finishing on the nano-indentation results. According to the literature sufficiently long chemomechanical polishing with alkaline colloidal silica is able to remove the damaged layers caused by mechanical polishing using diamond paste [20].

The mechanical properties, hardness (H) and elastic modulus (E), were measured using depth sensing nano/micro-indentation employing NANOVEA's mechanical tester. A Berkovich indenter and a maximum load of 400 mN were used for the nanonoindentation measurements whereas a Vickers indenter and a maximum load of 50 N were used for the micro-indentation. The calibration of the instrument was carried out employing fused silica (nano-indentation) and stainless steel sample (micro-indentation) and its calibration was verified by performing measurements on standard samples. For each test condition a minimum of ten indents spaced by 200 μm were performed in order to get statistically meaningful data. An optical microscope was used to select indented area free from visible defects.

During an indentation experiment an indenter of specified geometry, in our case a Berkovich indenter, penetrates into the surface of the material under investigation with constant loading rate. When the load reaches its set maximum value the indenter is held at this maximum load for a time period (holding time), and then the unloading takes place usually at the same rate with the loading. The load and penetration depth are measured versus time and these measurements are combined to give a load versus depth curve. The unloading part of the curves are analyzed following the method developed by Oliver and Pharr [21, 22] to obtain H and E.

For the W electromechanically polished sheet the hardness and elastic modulus were measured as a function of penetration depth (different maximum loads) for loading/unloading rate of 90 mN min^{-1} and holding time at a maximum load of 100 s. Also for this material the effect of loading/unloading rate and holding time at maximum load was investigated for the maximum load of 400 mN. This was performed in order to optimize the nano-indentation parameters and to investigate their effect on H and E values. Having shown that that there is no systematic dependence of the hardness and elastic modulus on these parameters, all W materials were measured for 400 mN maximum load, loading/unloading rate of 90 mN min^{-1} and holding time at a maximum load of 100 s.

3. Results and discussion

3.1. Microstructure

The microstructure of W sheet and W bar materials (with surface treatment that of W sheet A and forged W bar of table 1), as examined by SEM, is presented in figure 1. In the W sheet oriented grains mixed with arbitrarily distributed ones are observed. The direction along which most of the grains are elongated is presumably the rolling direction. The grain sizes were measured using image analysis software and the measurement of at least twenty grains. The visible grain size is in the range 1.4–4.4 μm in the rolling direction with an average value of 2.6 ± 0.9 μm and perpendicular to the rolling direction is in the range 0.6–2.7 μm with an average of 1.5 ± 0.6 μm. The W bar was fabricated by hammering on two orthogonal sides and therefore the grains are needle-like and are elongated along the bar axis. In figure 1(b) the surface normal of the sample is along the bar axis, and the grain size

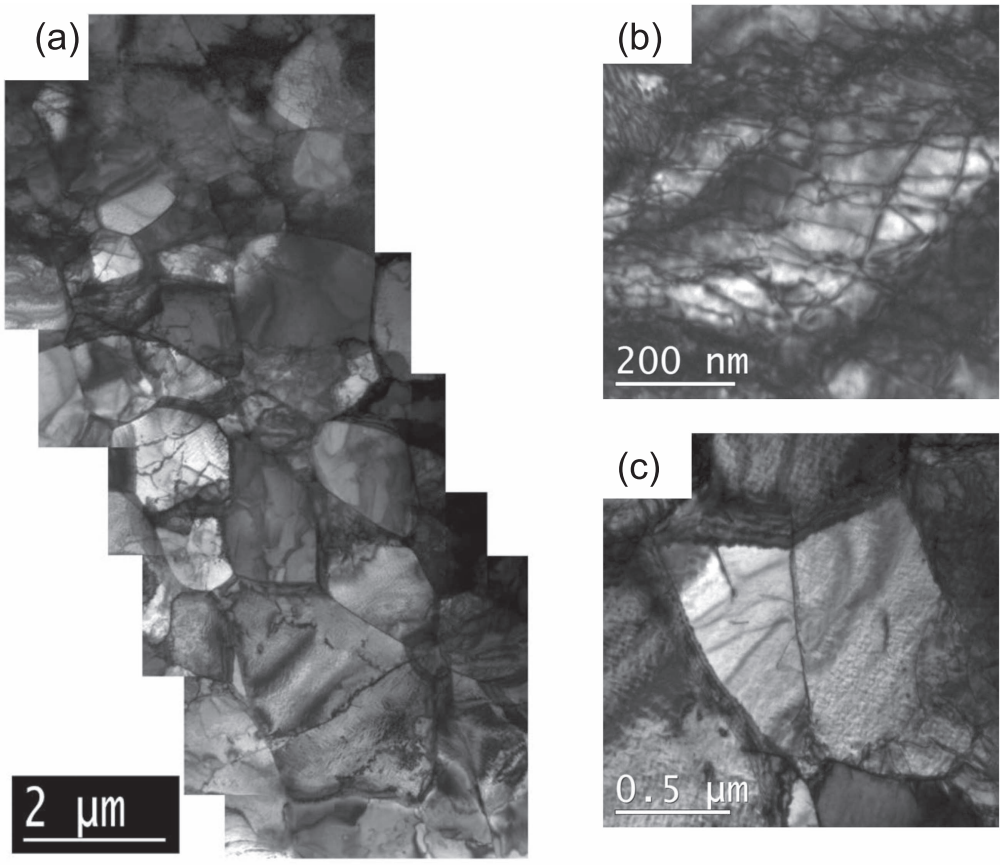

Figure 2. TEM images of the W sheet: (a) composite image in bright field, (b) dislocation network and (c) low angle grain boundaries.

perpendicular to this direction has an average value of $2.0 \pm 0.8\ \mu$m. The holes present in the W bar are due to the mechanical grinding and polishing of the material. It is noted that for the indentation measurements electropolishing was performed for adequate long time to ensure the removal of the damaged layers.

The TEM images of the W sheet and bar are presented in figures 2 and 3, respectively. These figures are composite images which are made by forming a puzzle of a number of TEM images. For the W sheet the visible sub-grain size is in the range 1.5–2 μm, while it presents a dense tangled dislocation network (figure 2(b)) with an average dislocation density of $(3.3 \pm 2.0) \times 10^{13}\ \mathrm{m}^{-2}$ and low angle grain boundaries (figure 2(c)). Regarding the W forged bar, due to the hammering of the bar from two orthogonal directions, the grains are needle-like and are elongated along the bar axis, as shown in figure 3. TEM measurements show that sub-grains are also elongated and their size varies in the range 0.6–1.7 μm and 2.3–4 μm, normal to and along the elongation directions, respectively. The dislocation density is about $(4–8) \times 10^{12}\ \mathrm{m}^{-2}$, depending on the particular sub-grain, and is being $(4.5 \pm 1.0) \times 10^{12}\ \mathrm{m}^{-2}$ on average.

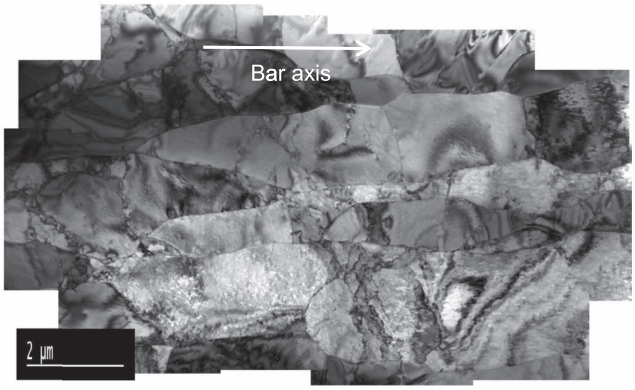

Figure 3. A composite TEM image of the forged W bar.

3.2. Indentation

The influence of the indentation depth on the obtained values of H and E was investigated for the chemomechanically polished W-sheet using different maximum loads, in the range 50–400 mN. The loading/unloading rate was kept at 90 mN min^{-1} and the holding time at maximum load at 100 s. Typical load—depth curves for three different maximum loads are presented in figure 4. For the investigated W samples no pop-in behavior [9] is observed at the beginning of the loading process (figure 4). It is noted that the imprint of the indent has as an edge size on each side varying between 3.3 and 12 μm for the maximum load of 50 and 400 mN, respectively, and for loads greater than 150 mN comprises several grains/sub-grains.

From the unloading part of the load-depth curves and assuming a power law for the load versus depth [19], the

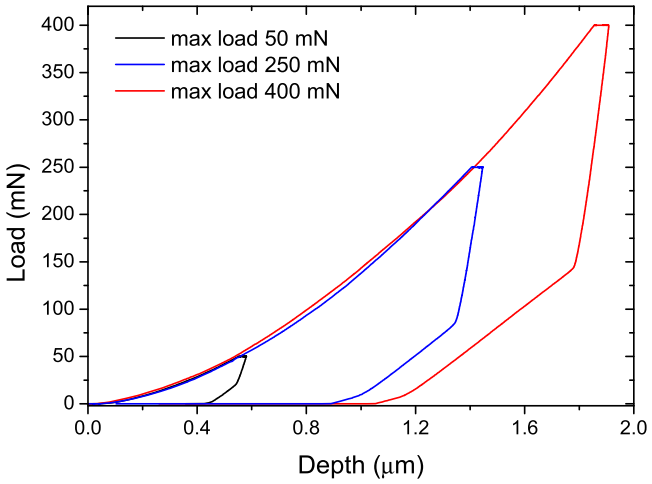

Figure 4. Load-depth curves for W sheet-A for three different maximum loads with loading/unloading rate of 90 mN min^{-1} and holding time at maximum load 100 s.

hardness and the elastic modulus were determined as a function of the penetration depth (figure 5).

It is observed that the hardness decreases as the penetration depth increases and after 1.2 μm it remains almost constant within error bars with an average value of $H_{av} = 5.9 \pm 0.2$ GPa (figure 5(a)). This behavior is understood by the well-known indentation size effect (ISE) [23], wherein the hardness is observed to increase with decreasing indentation size, especially in the sub-micrometer depth regime, and it is attributed to the evolution of geometrically necessary dislocations beneath the indenter, which gives rise to the strain gradients that cause enhanced hardening [24]. The derived value for H_{av} compares well with the average (in both directions, perpendicular and along the rolling direction) hardness of the 'cold rolled' W sheet reported by Reiser *et al* [25] and found to be 530 HV 0.1. The ISE effect has been found in previous studies of W material [26].

The application of the Nix–Gao formula ([22], solid line is figure 5(a))

$$\frac{H}{H_0} = \sqrt{1 + \frac{h^*}{h}}, \qquad (1)$$

where H is the hardness for a given depth, h, of indentation, H_0 is the hardness in the limit of infinite depth and h^* is a characteristic length that depends on the shape of the indenter, the shear modulus and H_0, gives $H_0 = 4.5 \pm 0.4$ GPa and $h^* = 1.13 \pm 0.38$ μm. The plot of the square of hardness versus the inverse of the indentation depth, h, at each load, shown in the inset of figure 5(a), reveals that a linear relation predicted by the Nix−Gao model agrees satisfactorily with the experimental results, within error bars, for depths larger than 0.8 μm.

The modified Nix–Gao model enables relating the characteristic length h^* with the dislocations statistically stored in the lattice, ρ_s, as [22, 27, 28]

$$\rho_s = \frac{3}{2}\frac{1}{f^3}\frac{\tan^2\theta}{bh^*}, \qquad (2)$$

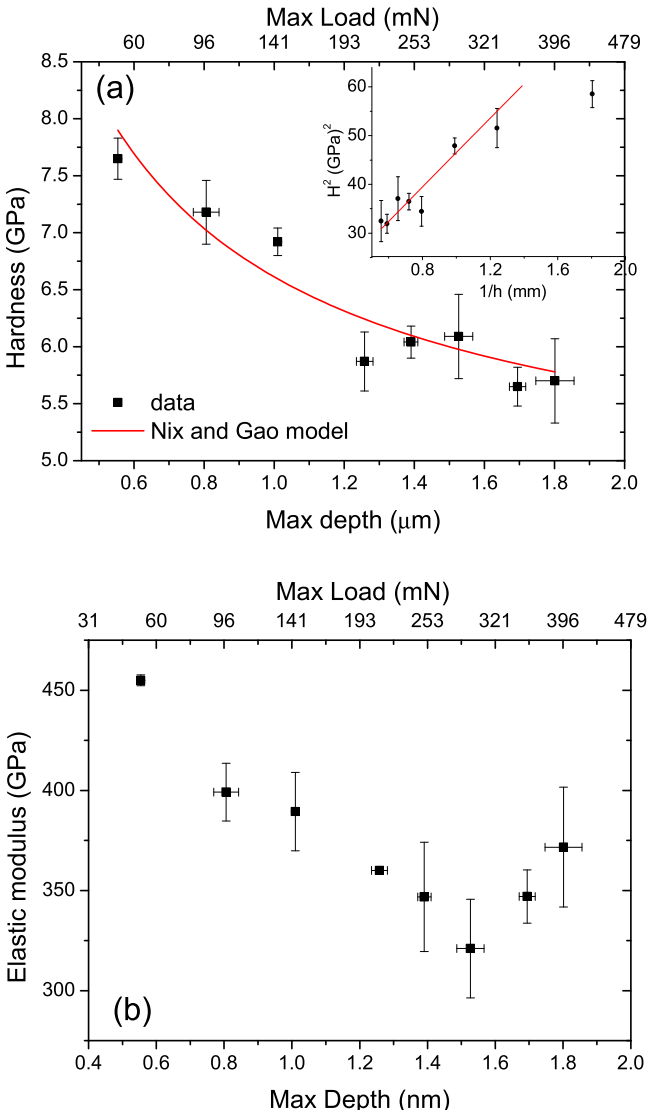

Figure 5. Hardness (a) and elastic modulus (b) as a function of penetration depth for W sheet-A. Inset (a): the hardness square as a function of inverse penetration depth.

where θ the angle between the surface of the material and the surface of the indenter, b the Burgers vector of the dislocations and f a correction factor for the size of the plastic zone [26]. In the present work $\tan\theta = 0.358$, $f = 1.9$ [26], and $b = 0.286$ nm. The application of equation (2) gives a dislocation density of 8.7×10^{13} m^{-2}. This value is in reasonable agreement with the dislocation density determined by TEM measurements, taking into account the error bar associated with TEM measurements.

The H_0 value agrees well with the Vickers hardness (440 HV) determined for this material by Wirtz *et al* [17].

The elastic modulus, E, as a function of penetration depth (figure 5(b)) shows a continuous decrease from 452 GPa at 0.5 μm depth to about 320 GPa at 1.5 μm depth and subsequently it slightly increases to 370 GPa for the maximum penetration depth of 1.8 μm. The decrease of E up to around 1.5 μm depth must be associated with the ISE as discussed above for the hardness behavior versus indentation depth. It is

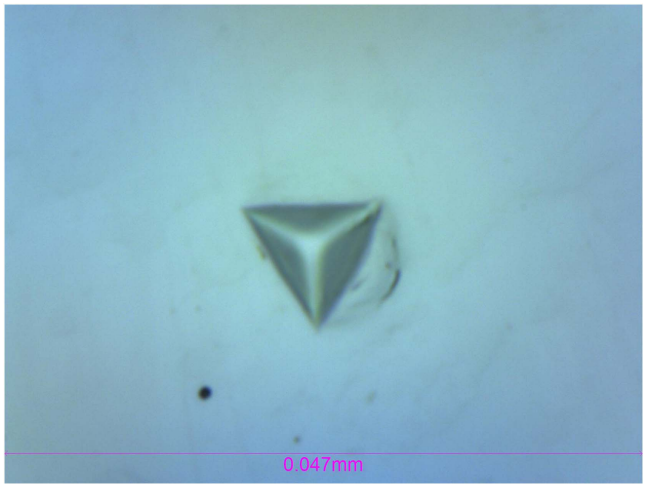

Figure 6. The imprint of the indent at 250 mN maximum load showing material pile-up effect.

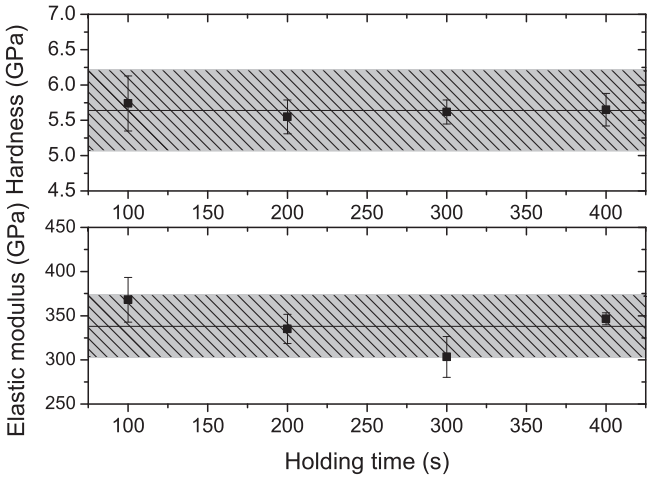

Figure 7. Hardness and elastic modulus versus holding time at the maximum load of 400 mN and for loading/unloading rate of 90 mN min^{-1} for W sheet-A.

known that, for a large range of materials, the hardness and elastic modulus, although they are distinct properties, increase together as it has been seen here. The increase of the elastic modulus for depths larger than about 1.5 μm could be attributed to the interaction between the plastically affected zone (PAZ) boundary and the grain/subgrain boundary. One may infer that at indentation depths around 1.5 μm the interaction between the PDZ boundary and the grain/subgrain boundary becomes dominating in the process of the indentation, which leads to the hindering of dislocation propagation and causes dislocation pile-up formation [25]. It is noted that for indentation depths larger than 1.5 μm, slight dislocation pile-up is observed around the imprint of the indents (see figure 6).

Furthermore, in order to assess the effect of the loading/unloading rate and the holding time at maximum load on hardness and elastic modulus, indentation tests were performed for various values of these parameters at the maximum load of 400 mN which corresponds to an indentation depth of about 1.8 μm. In figure 7 the hardness and elastic modulus variation versus holding time at the maximum load of 400 mN and for loading/unloading rate of 90 mN min^{-1} are depicted. The shaded area represents the 10% standard deviation of the average value (solid line in figure 7) of all the measurements. No significant variation is observed for the hardness and the elastic modulus, or in other words, the variation of the obtained values from their average is within 10%. The average values for H and E are 5.64 $\pm$ 0.08 GPa and 338 $\pm$ 27 GPa, respectively.

Regarding the loading rate effect on hardness and elastic modulus, only for the hardness a systematic slight increase in observed (figure 8), which must be associated with the strain hardening effect. As the loading rate increases the material becomes increasingly saturated with new dislocations, and more dislocations are prevented from nucleating, thus a resistance to dislocation-formation develops which manifests itself as a resistance to plastic deformation and increase of hardness. The average value of the elastic modulus is 345 $\pm$ 21 GPa which is in agreement with the average value

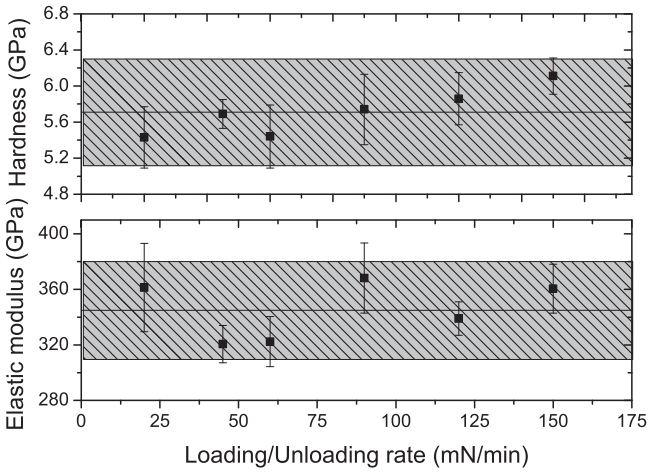

Figure 8. Hardness and elastic modulus versus loading/unloading rate for 400 mN maximum load and holding time 100 s for W sheet-A.

obtained for the different holding times at maximum load (figure 7).

Having shown above that there is no significant dependence of the hardness and elastic modulus on the loading/unloading rate and the holding time at the maximum load, the load-depth curves for the W materials under investigation were measured for 400 mN maximum load and for holding time and loading/unloading rate of 100 s and 90 mN min^{-1}, respectively (*supplementary file S1* is available online at stacks.iop.org/PSTOP/T170/014068/mmedia). It is noted that the penetration depth for 400 mN maximum load is around 1.8 μm and any surface effects are expected to be negligible.

The obtained values of hardness and elastic modulus for all the investigated materials at the maximum load of 400 mN, and for holding time and loading/unloading rate of 100 s and 90 nm min^{-1}, respectively, are presented in figure 9. Both electropolished and chemomechanically polished samples from the W sheet have the same hardness (5.7 $\pm$ 0.3 GPa),

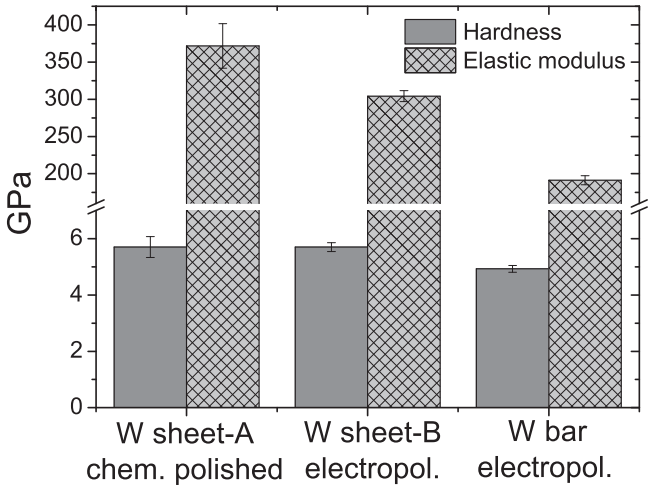

Figure 9. Hardness and elastic modulus for the various W materials for 400 mN maximum load, 100 s holding time and 90 mN min^{-1} loading/unloading rate.

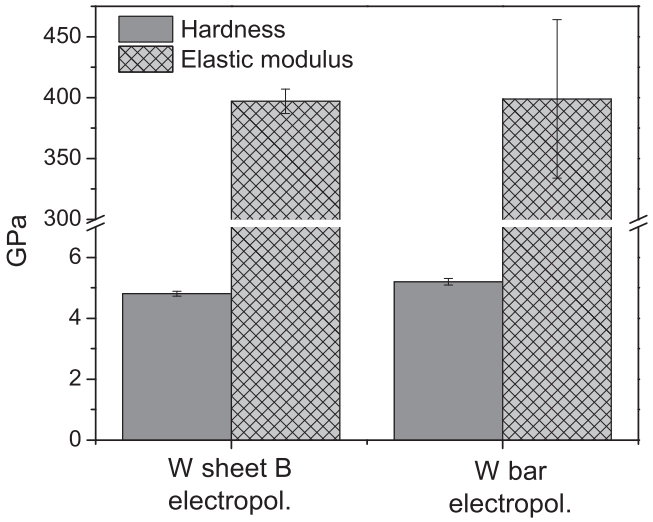

Figure 10. Hardness and elastic modulus for the various W materials for 50 N maximum load, 30 s holding time and 8 N min^{-1} loading/unloading rate.

indicating that the quality of the surface is equivalent for both. However, the hardness for the W bar is around 15% lower (4.9 ± 0.1 GPa). The higher hardness value of W sheet compared to W bar correlates with the higher dislocation density found by TEM in W sheet. The H value for the W bar is lower, by about 16%, than that determined by nano-indentation measurements in continuous stiffness mode [15]. Regarding the elastic modulus there is a considerable difference, outside the range of the statistical error bar, between W sheet chemomechanically polished and electropolished (figure 9). For the W bar the elastic modulus is 190 ± 6 GPa. The obtained value of E for the W sheet agrees very well with that of pure W produced by mechanical alloying and hot isostatic pressing which was determined employing nano-indentation and found to be 350 ± 40 GPa by Palacios *et al* [12] who investigated a tungsten material having a porosity of 9%. In general the presence of porosity in a material leads to lower *E* values.

The obtained values of elastic modulus differ significantly from that expected for W (390–410 GPa) [29]. For that reason micro-indentation measurements were carried out at larger depths of about 15 μm using a maximum load up to 50 N, 30 s holding time at maximum load and loading/unloading rate of 8 N min^{-1}. The obtained H and E values are depicted in figure 10. The elastic modulus for the W sheet is found 397 ± 10 GPa and for the W bar 399 ± 65 GPa, in agreement with literature values. Hardness is found a little lower than that determined using nano-indentation (4.8 ± 0.1 GPa for W sheet and 5.2 ± 0.1 GPa for W bar), but this is expected taking into account the behavior of *H* versus indentation depth (figure 5(a)). As the surface structure might be different than that of the bulk, absolute nano-mechanical values might not reflect the bulk material properties. Further, since for obtaining the elastic modulus in the nano-indentation few or possibly one grain participate, a large number indents are required for obtaining a representative average value. The results here demonstrate the importance of these considerations.

4. Summary

Two tungsten materials, namely a heavily deformed W sheet and a W forged bar, were investigated employing depth sensing nano-indentation and TEM measurements. The TEM measurements for the W sheet showed a sub-grain size the range 1.5–2 μm and an average dislocation density of (3.3 ± 2.0) × 10^{13} m^{-2} (figure 2). For the W bar the grain size is in the range 0.6–1.7 μm and 2.3–4 μm, normal to and along the elongation directions, respectively, and the average dislocation density (4.5 ± 1.0) × 10^{12} m^{-2} (figure 3). The hardness and elastic modulus for the W sheet were investigated as a function of the penetration depth using nano-indentation (figure 5). Hardness is found to follow the Nix–Gao model. The elastic modulus presents a minimum for penetration of 1.5 μm which might be explained by the interaction between the PAZ boundary and the grain/sub-grain interfaces. Moreover, it was found that the loading/unloading rate and the holding time at the maximum load do not have any significant influence on the obtained values of hardness and elastic modulus. The final surface treatment of the W material, either by electropolishing or chemomechanically polishing, results in the same hardness value of 5.7 ± 0.4 GPa. The W forged bar has a hardness of 4.9 ± 0.1 GPa as determined by nano-indentation. The discrepancy in nano-indentation hardness between W sheet and bar is attributed to dissimilar surface hardening effects during surface treatment, since when employing micro-indentation the hardness values are very close. The elastic modulus using nano-indentation gives much lower values than expected and when compared to micro-indentation. This effect is attributed to surface effects which influence the nano-indentation measurements as the penetration depth is much smaller (2 μm) compared to that of micro-indentation (15 μm). A neutron irradiation campaign of the same materials is underway at SCK · CEN, Belgium, at different irradiation doses and the

mechanical performance of the irradiated samples will be compared to that of the reference ones.

Acknowledgments

This work was carried out within the EUROfusion Consortium and received funding from the Euratom research and training programme 2014–2018 under grant agreement number No. 633053. The views and opinions expressed herein do not necessarily reflect those of the European Commission.

ORCID iDs

K Mergia https://orcid.org/0000-0002-2633-8750

References

[1] Wurster S *et al* 2013 *J. Nucl. Mater.* **442** S181–9
[2] Pintsuk G 2012 *Compr. Nucl. Mater.* **4** 551–81
[3] Geach G A and Hughes J R 1955 The alloys of rhenium and molybdenum or with tungsten and having good high temperature properties *Plansee Proc.* ed F Benesovsky (London: Pergamon) pp 245–53
[4] Rieth M, Reiser J, Dafferner B and Baumgärtner S 2012 *Fusion Sci. Technol.* **61** 381–4
[5] Kurishita H, Matsuo S, Arakawa H, Kobayashi S, Nakai K, Takida T, Takebe K and Kawai M 2008 *Mater. Sci. Eng.* A **477** 162–7
[6] Wei Q, Zhang H T, Schuster B E, Ramesh K T, Valiev R Z, Kecskes L J, Dowding R J, Magness L and Cho K 2006 *Acta Mater.* **54** 4079–89
[7] Riesch J, Buffiere J Y, Höschen T, Di Michiel M, Scheel M, Linsmeier C and You J H 2013 *Acta Mater.* **61** 7060–71
[8] http://euro-fusion.org/
[9] Fischer-Cripps A C 2011 *Nanoindentation* 3rd edn (New York: Springer)
[10] Pethica J B and Oliver W C 1989 *Mater. Res. Soc. Symp. Proc.* **130** 13–23
[11] Syed Asif S A and Pethica J B 1997 *Phil. Mag.* A **76** 1105–18
[12] Terentyev D, Bakaeva A, Pardoen T, Favache A and Zhurkin E E 2016 *J. Nucl. Mater.* **476** 1–4
[13] Palacios T, Jiménez A, Muñóz A, Monge M A, Ballesteros C and Pastor J Y 2014 *J. Nucl. Mater.* **454** 455–61
[14] Dubinko A, Terentyev D, Bakaeva A, Pardoen T, Zibrov M and Morgan T W 2017 *Nucl. Instrum. Methods Phys. Res.* B **393** 155–9
[15] Dubinko A, Terentyev D, Bakaeva A, Verbeken K, Wirtz M and Hernández-Mayoral M 2017 *Int. J. Refract. Hard Met.* **66** 105–15
[16] Reiser J, Hoffmann J, Jäntsch U, Klimenkov M, Bonk S, Bonnekoh C, Hoffmann A, Mrotzek T and Rieth 2017 *Int. J. Refract. Hard Met.* **64** 261–78
[17] Wirtz M, Uytdenhouwen I, Barabash V, Escourbiac F, Hirai T, Linke J, Loewenhoff T, Panayotis S and Pintsuk G 2017 *Nucl. Fusion* **57** 066018
[18] Bonk S, Reiser J, Hoffmann J and Hoffmann A 2016 *Int. J. Refract. Hard Met.* **60** 92–8
[19] Hirsch P, Howie A, Nicholson R, Pashley D W and Whelan M J 1997 *Microscopy of Thin Crystals* (Florida: Krieger Publishing Company Malabar)
[20] Manhard A, Matern G and Balden M 2013 *Prakt. Metallogr.* **50** 5–16
[21] Oliver W C and Pharr G M 1992 *J. Mater. Res.* **7** 1564–83
[22] Oliver W and Pharr G 2004 *J. Mater. Res.* **19** 3–20
[23] Nix W D and Gao H 1998 *J. Mech. Phys. Solids* **46** 411–25
[24] Rester M, Motz C and Pippan R 2009 *J. Mater. Res.* **24** 647–51
[25] Reiser J, Hoffmann J, Jäntsch U, Klimenkov M, Bonk S, Bonnekoh C, Rieth M, Hoffmann A and Mrotzek T 2016 *Int. J. Refract. Hard Met.* **54** 351–69
[26] Liu G-Y, Ni S and Song M 2015 *Trans. Nonferrous Met. Soc. China* **25** 3240–6
[27] Durst K, Backes B and Mathias G 2005 *Scr. Mater.* **52** 1093–7
[28] S Graça S, Colaço R, Carvalho P A and Vilar R 2008 *Mater. Lett.* **62** 3812–4
[29] Lassner E and Schubert W-D 1999 *Tungsten: Properties, Chemistry, Technology of the Element, Alloys, and Chemical Compounds* (New York: Kluwer) p 18